BIOCHEMISTRY
including biophysical chemistry & molecular biology

ACS AuthorChoice

Article

pubs.acs.org/biochemistry

Perturbation of the Monomer−Monomer Interfaces of the Benzoylformate Decarboxylase Tetramer

Forest H. Andrews,[†] Megan P. Rogers,[†] Lake N. Paul,[‡] and Michael J. McLeish*,[†]

[†]Department of Chemistry and Chemical Biology, Indiana University-Purdue University Indianapolis, Indianapolis, Indiana 46202, United States

[‡]Bindley Biosciences Center, Discovery Park, Purdue University, West Lafayette, Indiana 47904, United States

Supporting Information

ABSTRACT: The X-ray structure of benzoylformate decarboxylase (BFDC) from *Pseudomonas putida* ATCC 12633 shows it to be a tetramer. This was believed to be typical of all thiamin diphosphate-dependent decarboxylases until recently when the structure of KdcA, a branched-chain 2-keto acid decarboxylase from *Lactococcus lactis*, showed it to be a homodimer. This lent credence to earlier unfolding experiments on pyruvate decarboxylase from *Saccharomyces cerevisiae* that indicated that it might be active as a dimer. To investigate this possibility in BFDC, we sought to shift the equilibrium toward dimer formation. Point mutations were made in the noncatalytic monomer−monomer interfaces, but these had a minimal effect on both tetramer formation and catalytic activity. Subsequently, the R141E/Y288A/A306F variant was shown by analytical ultracentrifugation to be partially dimeric. It was also found to be catalytically inactive. Further experiments revealed that just two mutations, R141E and A306F, were sufficient to markedly alter the dimer−tetramer equilibrium and to provide an ∼450-fold decrease in k_{cat}. Equilibrium denaturation studies suggested that the residual activity was possibly due to the presence of residual tetramer. The structures of the R141E and A306F variants, determined to <1.5 Å resolution, hinted that disruption of the monomer interfaces will be accompanied by movement of a loop containing Leu109 and Leu110. As these residues contribute to the hydrophobicity of the active site and the correct positioning of the substrate, it seems that tetramer formation may well be critical to the catalytic activity of BFDC.

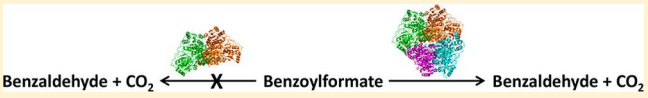

Oligomerization of proteins in biological systems is a common phenomenon, and protein−protein interactions are often involved in critical cellular processes. The destabilization of interfaces in multimeric protein complexes is thought to contribute to diseases ranging from neurodegenerative disorders to muscular dystrophy.[1−3] Because proteins rarely act alone *in vivo*, predicting networks of protein−protein interactions, i.e., the "interactome", has become fundamental to the development of systems biology.[4−6] As a consequence, predicting how any given protein will interact with other biomolecules, understanding the forces stabilizing protein−protein interfaces, and learning how to destabilize an individual interface have become the focus of much research.[7−9]

One of the most common protein−protein interactions is self-association.[10,11] In essence, this allows a single gene of relatively short length to encode a large protein system by allowing multiple peptide sequences encoded from that gene to interact and form a large multimeric protein. In addition to a reduced genome and fewer problems with transcription, this system provides benefits such as an increase in the effective concentration within the cell, enhanced protein stability, and additional regulatory flexibility.[11] While self-association is not necessarily a prerequisite for activity, the active sites of perhaps one-sixth of all oligomeric enzymes are located at highly stabilized interfaces between two peptide chains.[11]

Such is the case with thiamin diphosphate (ThDP)-dependent enzymes.[12,13] While this group of enzymes has evolved to catalyze a wide range of chemical reactions,[14] X-ray structures have shown that overwhelmingly they have developed only one way to bind the ThDP cofactor, namely at the interface between two monomers. This creates two active sites per homodimer with each monomer contributing either a pyrimidine binding (PYR) domain or a diphosphate binding (PP) domain to a given active site (Figure 1). At a minimum, therefore, any ThDP-dependent enzyme must form a dimer.[12,13] Curiously, until recently, all the ThDP-dependent enzymes whose sole *in vivo* function is to catalyze a decarboxylation reaction were found to be homotetramers, albeit more accurately described as dimers of active dimers.[15−21] The branched-chain 2-keto acid decarboxylase from *Lactococcus lactis* (KdcA, EC 4.1.1.72) was the first to deviate from this trend when its X-ray structure [Protein Data Bank (PDB) entry 2VBG] showed to it be dimeric.[22] Intriguingly, although the archetypal ThDP-dependent decarboxylase, pyruvate decarboxylase from *Saccharomyces cerevisiae* (*Sc*PDC, EC 4.1.1.1), is a tetramer in the crystal lattice, analytical ultracentrifugation (AUC) experiments showed it to be a dimer at low solution concentrations.[23] Further, using urea as a denaturant, it was possible to shift the dimer−tetramer equilibrium in favor of the dimer and to demonstrate that the dimer was catalytically active.[24,25]

Received: January 20, 2014
Revised: May 18, 2014
Published: June 23, 2014

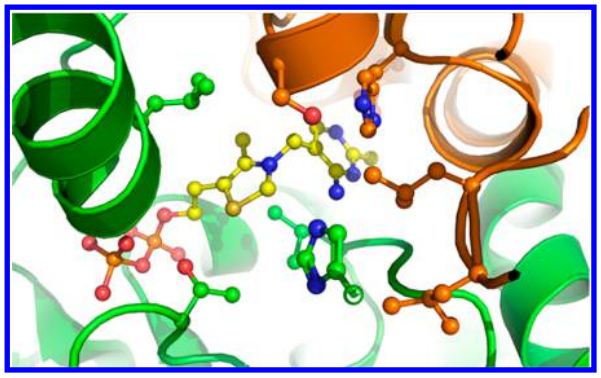

Figure 1. ThDP (yellow) in the active site of BFDC. The cofactor interacts with both the phosphate-binding domain of monomer A (green) and the pyrimidine-binding domain of monomer B (orange). Prepared using PyMOL using data from PDB entry 1BFD.

Benzoylformate decarboxylase (BFDC, EC 4.1.1.7) is another ThDP-dependent decarboxylase that has been shown to be a homotetramer.[18] First identified as part of the mandelate pathway of *Pseudomonas putida*,[26] BFDC catalyzes the non-oxidative decarboxylation of benzoylformate to yield benzaldehyde and carbon dioxide.[27] Not surprisingly, given the similarity of their reactions, there is considerable structural homology between BFDC and PDC, including the conservation of several catalytic residues. As part of a project examining the evolution of ThDP-dependent enzymes, we have been attempting to interconvert the two enzymes, but with limited success.[28,29] Unlike *Sc*PDC, it has never been determined whether BFDC is active as a dimer, nor has it been shown what advantage, if any, the tetramer provides to BFDC. Here, we report the use of site-directed mutagenesis coupled with analytical centrifugation and X-ray crystallography to answer two questions. (i) Can BFDC be converted into a dimer? (ii) Is the tetramer required for enzymatic activity?

MATERIALS AND METHODS

Primers were synthesized by Integrated DNA Technologies. Recombinant alcohol dehydrogenase from *Equus caballus* (HLADH) was obtained as described previously.[30] Reduced β-nicotinamide adenine dinucleotide (NADH), isopropyl β-D-thiogalactopyranoside (IPTG), and benzoylformate were purchased from Sigma-Aldrich. A gel filtration calibration kit (high molecular mass) and HiPrep 16/60 Sephacryl S-200 High Resolution column were purchased from GE Healthcare. Nickel-nitrilotriacetic acid (NTA) resin was purchased from Qiagen. *Pfu* DNA polymerase was purchased from Stratagene. Buffers and other assay reagents were purchased from either Sigma-Aldrich or Fisher Scientific and were of the highest grade commercially available. Sequencing was conducted by the University of Michigan DNA Sequencing Core Facility.

Analysis of Dimer and Tetramer Interfaces. The X-ray structure of *wt* BFDC at 1.60 Å resolution (PDB entry 1BFD) was used as the model for analysis of the interfaces. The SPPIDER server (http://sppider.cchmc.org) was used to calculate the total surface area and the interface surface area and to verify that residues selected for mutagenesis were not involved in the formation of the active dimer. The PDB visualization program PyMOL (Schrödinger, LLC) was used to identify targets for mutagenesis and for the preparation of figures.

Plasmids. Mutagenesis was performed on BFDC expression vector pET24dBFDC-His.[31,32] Primers (Table 1 of the Supporting Information) were designed, and site-directed mutagenesis was performed according to the QuikChange mutagenesis protocol (Agilent) utilizing *Pfu* DNA polymerase. DpnI was used to digest parental DNA prior to its transformation into chemically competent TOP10 cells. Each plasmid used for protein expression had the complete *mdlC* gene sequenced to ensure that only the desired mutations were present.

Protein Expression and Purification. Expression of *wt* BFDC and its variants was conducted in *Escherichia coli* strain BL21(DE3). Induction of the recombinant protein was initiated with 1 mM IPTG. Following induction, the cultures were grown at room temperature overnight (18−20 h). Enzymes were purified as described previously.[31] The protein was exchanged into BFDC storage buffer [100 mM $KHPO_4$, 1 mM $MgSO_4$, 0.5 mM ThDP (pH 6.0), and 10% (v/v) glycerol] and concentrated using Amicon Ultra centrifugal filters (Millipore). Purity was assessed by sodium dodecyl sulfate−polyacrylamide gel electrophoresis, and the protein concentration was determined from the absorbance at 280 nm using a molar extinction coefficient of 62220, calculated from the sequence of *wt* BFDC with the ExPASy ProtParam tool.[33] Enzymes were stored at −80 °C until they were required.

Steady-State Kinetic Analysis of Wild-Type and Variant BFDC. The coupled activity assay of the purified enzymes was performed as described previously.[34] The assay mixture contained bovine serum albumin (BSA, 1 mg/mL), NADH, and HLADH in 100 mM potassium phosphate buffer (pH 6.0), and varying concentrations of benzoylformate in a final volume of 1 mL. Reactions were conducted at 30 °C and were initiated by the addition of the enzyme. Assays were performed in triplicate. Steady-state kinetic parameters were determined by fitting the initial rate data to the Michaelis−Menten equation, using the enzyme kinetics module of SigmaPlot version 9.0.1 (Systat Software, Inc.).

For the equilibrium denaturation studies, assays were conducted in denaturation buffer using the direct UV assay of Hegeman.[26] The decrease in benzoylformate concentration was monitored at 334 nm.

Molecular Mass Predicted by Size-Exclusion Chromatography (SEC). Size-exclusion chromatography (SEC) was performed using an AKTA fast performance liquid chromatography system (GE Healthcare) equipped with a HiPrep 16/60 Sephacryl S-200 High Resolution column (1.6 cm × 94 cm). The column was equilibrated with running buffer [50 mM $NaPO_4$ and 150 mM NaCl (pH 7.5)] prior to calibration. Blue Dextran was used to determine the void volume of the column. A standard curve was obtained using a high-molecular mass gel filtration calibration kit (GE Healthcare). Protein standards were loaded according to the manufacturer's protocol. BFDC variants were loaded onto the column via injection into a 2 mL loop at concentrations ranging from 0.1 to 1 mg/mL in a total volume of 400 μL. K_{av} values were calculated and used to predict the molecular mass and oligomerization state of the BFDC variants

SEC-MALS Analysis. Size-exclusion chromatography multi-angle light scattering (SEC-MALS) was performed on *wt* BFDC and the R141E/A306F and R141E/Y288A/A306F variants. Three concentrations, 3.1, 1.5, and 0.75 mg/mL, were used for the mutant BFDC proteins. For the *wt* enzyme, concentrations of 2.0, 1.0, and 0.75 mg/mL were used. A Superdex 200 column coupled to the three-angle miniDawn TREOS and Optilab-Trex instrument (Wyatt Technologies) was used for collection of the light scattering and refractive index data. The system is coupled to an Agilent 1100 high-performance liquid chromatography

dx.doi.org/10.1021/bi500081r | *Biochemistry* 2014, 53, 4358−4367

system at a flow rate of 0.45 mL/min with an in-line spectrophotometer. Astra (version 6.0.3) was used to analyze the collected data.

Analytical Ultracentrifugation. Sedimentation velocity experiments were conducted on Beckman-Coulter XLA and XLI analytical ultracentrifuges. *wt* BFDC and the R141E/A306F and R141E/Y288A/A306F variants were dialyzed extensively against a buffer containing 100 mM $NaPO_4$ (pH 7.5), 300 mM NaCl, 1 mM $MgCl_2$, and 35 μM ThDP. The sample concentrations ranged from 0.25 to 1.0 mg/mL. The samples were then centrifuged at 42000 rpm using two-sector 1.2 cm path-length carbon-filled Epon centerpieces. The experiments were conducted on an An-50 Ti rotor at 20 °C. The density and relative viscosity of the buffers were calculated with SEDNTERP version 1.09 (http://www.jphilo.mailway.com/download.htm#SEDNTERP) to be 1.01949 g mL^{-1} and 0.01069 P, respectively. On the basis of its sequence, the partial specific volume (vbar) of the protein was calculated with SEDNTERP to be 0.7340 mL g^{-1}. The samples were monitored at 280 nm with a 4 min delay and 150 scans. The $c(s)$ distributions were analyzed using SEDFIT version 14.3e.[35] Molecular masses were calculated from the $c(s)$ data using a shape assumption.

Urea Unfolding Monitored by Circular Dichroism (CD) Spectroscopy and Fluorescence Spectrophotometry. *wt* BFDC and the R141E/A306F variant (0.15 mg/mL) were incubated overnight at 4 °C with varying urea concentrations in 50 mM phosphate buffer (pH 6.0). Far-UV CD experiments were conducted on a Jasco J-810 spectropolarimeter. Unfolding was monitored by changes in ellipticity at 222 nm in a cell with a path length of 0.1 cm at 20 °C. Spectra were averaged over five scans, and the scan speed was set at 20 nm/min with a response time of 1 s and a slit width of 1 nm.

Fluorescence emission spectra were recorded on a Varian Cary Eclipse fluorescence spectrophotometer. The intrinsic fluorescence of *wt* BFDC and the R141E/A306F variant, both at 0.15 mg/mL in varying concentrations of urea in 50 mM phosphate buffer (pH 6.0) at 20 °C, was recorded from 295 to 450 nm using an excitation wavelength of 280 nm. The bandpass for excitation and emission was set at 5 nm with a scanning rate of 200 nm/min.

Crystallization of the R141E and A306F Variants. Crystals of BFDC R141E and BFDC A306F variants were grown by the hanging drop diffusion method under the same conditions used for the crystallization of *wt* BFDC.[18] Storage buffer was exchanged for crystallization buffer [0.1 mM $MgCl_2$, 0.2 mM ThDP, and 25 mM NaHEPES (pH 7.0)]. The well solution consisted of 0.1 M Tris (pH 8.5), 0.15 M $CaCl_2$, and 22% PEG400 (v/v). Equal volumes of protein (10 mg/mL) and well solution were pipetted onto a silanized glass slide and mixed. A heavy precipitate immediately formed from this mixture, and single crystals emerged from the precipitate within days. Crystals were transferred to fresh crystallization buffer containing 36% (v/v) glycerol as a cryoprotectant and mounted on Hampton CryoLoops immediately prior to being flash-frozen in liquid nitrogen.

X-ray Data Collection. Diffraction data were obtained at 100 K on the 23-ID-D and 23-ID-B beamlines administered by GM/CA-CAT at the Advanced Photon Source at Argonne National Laboratory (Argonne, IL). Data sets for the R141E and A306F variants were scaled to the I_{222} space group. Data reduction and processing of data sets were achieved using the HKL2000 software package and the CCP4 suite of programs.[36] Molecular replacement was performed using the search model *wt* BFDC (PDB entry 1BFD) with metals and waters removed. The asymmetric unit for each variant contained a single monomer.

Structure Solutions and Refinements. PHENIX was used for model refinement.[37] After each round of refinement, the electron density was manually inspected and models were built using Coot.[38] Refinement continued until R_{free} and the crystallographic R factor could no longer be improved. The validity of the model was checked using the MolProbity server.[39] All images were generated using PyMOL (Schrödinger, LLC).

RESULTS

Comparison of the Quaternary Structures of KdcA, *Sc*PDC, and BFDC. It is clear from their respective X-ray structures that KdcA[22] is a homodimer and that BFDC[18] is a homotetramer (Figure 2). Although *Sc*PDC was initially

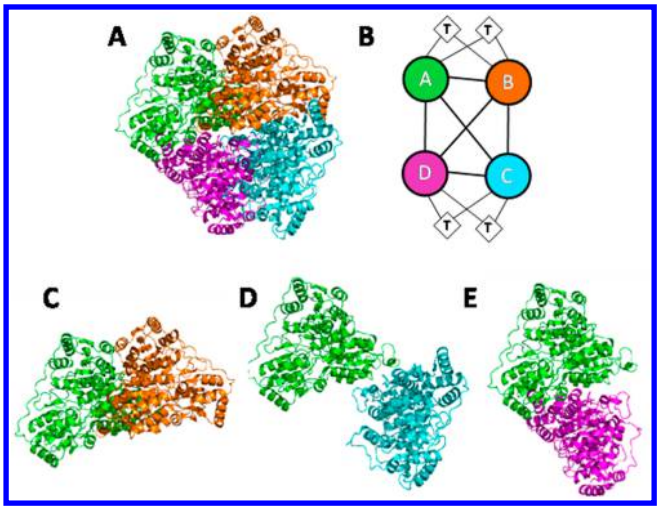

Figure 2. Defining the interfaces of BFDC monomers. (A) BFDC tetramer. Monomer A is colored green, monomer B orange, monomer C cyan, and monomer D magenta. (B) Cartoon with lines indicating interactions between the monomers (circles) and ThDP (diamonds). The active sites (one per monomer) are found at the A–B interface. (C–E) A–B, A–C, and A–D interfaces, respectively. Figures based on data from PDB entry 1BFD.

reported to be a homotetramer,[40] structural analysis suggests that its tetrameric form may arise simply by crystal packing.[40] To examine this possibility, we turned to the Solvent accessibility-based Protein-Protein Interface iDEntification and Recognition (SPPIDER) server that can be used to predict the total surface area of interfaces from a PDB file.[41] Analyses were conducted on three ThDP-dependent decarboxylases, KdcA (PDB entry 2VBF), *Sc*PDC (PDB entry 1PYD), and BFDC (PDB entry 1BFD). In each case, the interface forming the active site, defined as the A–B interface (Figure 2), was clearly identified (Table 1). There was no evidence of any dimer–dimer interface in the KdcA structure, supporting the crystallographic finding of a homodimer. Interestingly, no evidence was found for any dimer–dimer interface when the *Sc*PDC structure was used as the search model. This reinforces the suggestion that the tetramer observed in the crystal lattice of *Sc*PDC might be an artifact of protein crowding at higher enzyme concentrations. Conversely, analysis of the X-ray structure of BFDC with SPPIDER indicates a robust dimer–dimer interface accounting for almost 10% of the total surface are of the enzyme (Table 1).

Analysis of the Dimer–Dimer Interfaces of BFDC. SPPIDER analysis of the quaternary structure of BFDC shows

Table 1. SPPIDER Analysis of Monomer−Monomer Interfaces[a]

interface	KdcA surface area (Å^2)	*Sc*PDC surface area (Å^2)	BFDC surface area (Å^2)	*Zm*PDC surface area (Å^2)
monomer	21856	21819	20611	22364
chain A−chain B	3458 (16%)	2819 (13%)	3475 (17%)	4204 (19%)
chain A−chain C	nd[b]	nd[b]	488 (2%)	611 (3%)
chain A−chain D	nd[b]	nd[b]	1601 (8%)	1226 (5%)

[a]Surface areas were calculated from PDB entries 2VBF (KdcA), 1PYD (*Sc*PDC), 1BFD (BFDC), and 1ZPD (*Zm*PDC) using the SPPIDER server. [b]No interface can be detected by SPPIDER.

that each chain has significant interactions with every other chain in the tetramer (Table 1). The interface that forms the active dimer, the A−B interface, was calculated to have the largest total area of contact (3540 Å^2), ∼17% of the solvent accessible surface area of the monomer. It seems logical that disruption of the A−B interface would result in a loss of enzyme activity; therefore, our attempts to convert BFDC into a dimer were focused on disrupting the A−C and A−D interfaces (Figure 2).

The A/D interface was the next largest, with a total surface area of ∼1600 Å^2 or about 8% of the total monomer A surface area. Here Tyr288 and Ala306 were identified as possible candidates for mutagenesis. Tyr288 of monomer A has 12 points of contact within 5 Å of monomer D (Figure 3), and it was reasoned that

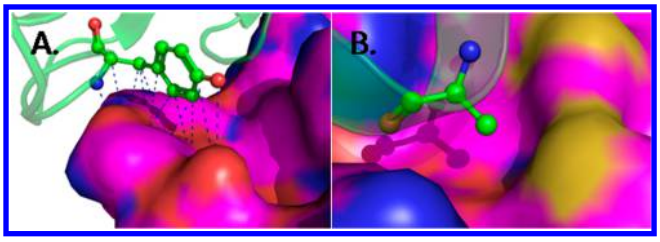

Figure 3. Interactions at the A−D interface. (A) Tyr288 of monomer A is found to have 12 points of contact (≤5 Å) with monomer D. (B) Ala306 of monomer A is located in a shallow hydrophobic cleft of monomer D.

elimination of most of these interactions by removal of the phenyl ring should result in a less stable A/D interface. Additionally, the methyl side chain of Ala306 on monomer A is located in a shallow hydrophobic cleft of monomer D (Figure 3), and it was thought that replacement by a bulkier residue such as phenylalanine would not be tolerated, and may help disrupt the interface.

At ∼500 Å^2, the A−C interface accounts for ∼2.5% of the total surface area of monomer A and is mostly comprised of residues in charge−charge interactions. The side chains of Glu107 and Asp114 of monomer A, for example, form salt bridges with Arg141 and Arg120, respectively, of monomer C (Figure 4). Because of the 2-fold symmetry, Arg120 and Arg141 of monomer A also interact with Asp114 and Glu107 of monomer C. These four positions were selected as targets for mutagenesis, specifically to introduce like-charge repulsions in an attempt to destabilize the dimer−dimer interface. A summary of the various interactions, and the rationale for the mutagenesis experiments can be found in Table S2 of the Supporting Information.

Kinetic and SEC Analysis of A−C and A−D Single-Mutation Variants. All variants expressed as soluble protein.

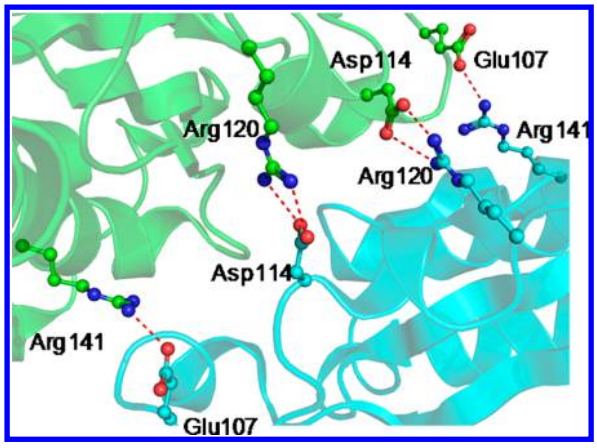

Figure 4. Interactions at the A−C interface. View of charged residues highlighting those with interatomic distances of ∼3 Å.

Using the typical assay conditions described in Materials and Methods, K_m and k_{cat} values of the A−D variants were very similar to those of *wt* BFDC (Table 2). The A−C variants also exhibited no change in their K_m values, but compared to that of *wt* BFDC, there was a modest 2−4-fold decrease in their k_{cat} values. All variants eluted from the SEC column at a volume indicative of a tetramer (Table 2). On the basis of these results, it appeared that the single mutations did not noticeably alter the dimer−tetramer equilibrium or greatly affect the overall catalytic activity of the enzyme.

Generation and Analysis of the R141E/Y288A/A306F Variant. The inability of a single mutation to produce a dimeric BFDC prompted a reanalysis of the A−D and A−C interfaces. The A−D interface accounts for nearly 10% of the total surface area; therefore, it was not surprising that more than one unfavorable interaction would be required to disrupt it. It was noted that the hydrophobic pocket that accommodates Ala306 comprised Met145, Met148, and the hydrophobic region of the Arg141 side chain. It was reasoned that replacement of Arg141 with a glutamic acid would have a dual effect in that it would set up an unfavorable interaction with Glu107 and reduce the hydrophobicity of the Ala306 binding pocket. To maximize the destabilizing interactions, the R141E/Y288A/A306F variant was constructed. The triple mutant expressed well and was purified as a soluble protein. When subjected to SEC chromatography at 1 mg/mL, it eluted at a volume similar to that of *wt* BFDC but, at ≤0.5 mg/mL, it eluted at a larger volume, suggestive of a change in oligomerization state (Table 2). Unfortunately, it also was inactive in the assay.

Verification of the Quaternary Structure of *wt* BFDC and the R141E/Y288A/A306F Variant. To validate the SEC observations and to confirm that the oligomerization state of the triple mutant was indeed concentration-dependent, we turned to a combination of analytical ultracentrifugation and SEC-MALS. Sedimentation velocity experiments were performed, and the sedimentation coefficients (S) for *wt* BFDC were determined at concentrations of 0.25, 0.5, and 1.0 mg/mL (Figure S1 of the Supporting Information). At each concentration, an S value of 8.4 was calculated from a $c(s)$ distribution (Table S3 of the Supporting Information). The calculated molecular mass from these experiments was 241 ± 22 kDa, which agrees with the theoretical molecular mass of ∼229 kDa for the BFDC tetramer. Additional SEC-MALS analysis provided a molecular mass of 235.1 ± 16.5 kDa, also corresponding to a tetrameric species (Table S4 of the Supporting Information). Similar experiments

dx.doi.org/10.1021/bi500081r | *Biochemistry* 2014, 53, 4358−4367

Table 2. Steady-State Kinetic Parameters[a,b] and Oligomerization States[c] of the BFDC Variants

variant	k_{cat} (s^{-1})[b]	K_m (mM)	k_{cat}/K_m (mM^{-1} s^{-1})[b]	oligomerization state at ≤0.5 mg/mL
wt BFDC	350 ± 30 (1)	0.30 ± 0.03	1200 (1)	tetramer
Y288A	310 ± 20 (1)	0.25 ± 0.03	1200 (1)	tetramer
A306F	250 ± 23 (1)	0.31 ± 0.09	890 (1.3)	tetramer
R141E	180 ± 22 (2)	0.19 ± 0.05	950 (1.3)	tetramer
R120E	130 ± 26 (3)	0.29 ± 0.10	450 (2.7)	tetramer
E107R	130 ± 10 (3)	0.33 ± 0.10	390 (3)	tetramer
D114R	83 ± 12 (4)	0.25 ± 0.10	330 (3.6)	tetramer
E107R/D114R	0.8 ± 0.04 (440)	0.35 ± 0.05	2 (585)	tetramer
R141E/Y288A	15 ± 2 (23)	0.21 ± 0.03	70 (17)	tetramer
R141E/A306F	0.8 ± 0.3 (440)	0.25 ± 0.02	3 (400)	evidence of dissociation
Y288A/A306F	0.1 ± 0.01 (3500)	0.33 ± 0.03	0.3 (4000)	tetramer
R141E/Y288A/A306F	nad[d]	nad[d]	nad[d]	evidence of dissociation
L109A	3.9 ± 0.3 (90)	0.80 ± 0.1	4.8 (250)	nd[e]
L110A	1.5 ± 0.3 (230)	2.8 ± 0.3	0.5 (2400)	nd[e]

[a]Values are means of three independent determinations ± the standard error (SE). All variants were prepared with C-terminal hexahistidine tags and assayed as described in Materials and Methods. [b]In parentheses are fold decreases over the *wt* value. [c]Oligomerization states for variants were determined by SEC as described in Materials and Methods. [d]No activity detected. [e]Not determined.

were performed on the triple mutant, and by contrast, the *S* value determined at the same concentrations was found to be 7.9 (Figure S1 of the Supporting Information). The SEC-MALS analysis for the R141E/Y288A/A306F variant showed a pronounced concentration-dependent shift in both molecular mass and retention time (Figure S2 and Table S4 of the Supporting Information). All these changes pointed to a shift in the dimer−tetramer equilibrium.

Analysis of the R141E/Y288A/A306F Permutation Variants. Having seemingly changed the dimer−tetramer equilibrium, we thought it was important to determine which combination of mutations was crucial in bringing about the change. Accordingly, the three permutations of the R141E/Y288A/A306F mutant were constructed. Once again, the variants were expressed as soluble proteins and could be assayed under standard conditions. Like the single mutants, R141E/Y288A, R141E/A306F, and Y288A/A306F variants all had K_m values similar to that of *wt* BFDC. Conversely, they all showed considerable decreases in k_{cat} values, with the greatest decrease (~3500-fold) seen for Y288A/A306F (Table 2). Each of the variants was subjected to SEC chromatography at concentrations ranging from 0.1 to 1 mg/mL. While R141E/Y288A and Y288A/A306F eluted at volumes indicative of a tetramer regardless of concentration, the R141E/A306F variant exhibited concentration-dependent changes similar to those shown previously by the R141E/Y288A/A306F variant. In some ways, this was a surprising result as the k_{cat} value for R141E/A306F was 0.8 s^{-1}, admittedly a ~450-fold decrease over that of *wt* BFDC but still much higher than that of the Y288A/A306F variant that remained a tetramer. The Y288A and A306F single variants retained nearly wild-type activity (Table 2), so it is not unreasonable to assume that the double mutant exhibiting the greatest decrease in activity would be the one most likely to show alterations in its oligomerization state. Clearly, that is not the case here, and the reasons for the reduced activity in this variant will become the focus of a future investigation.

To explore this further, the R141E/A306F variant was analyzed, in turn, by analytical centrifugation (Figure S1 of the Supporting Information) and SEC-MALS (Figure S2 of the Supporting Information). The calculated *S* value for the double mutant was 7.3, significantly lower than that of *wt* BFDC. This number was obtained at all protein concentrations (Table S3 of the Supporting Information). It was also apparent from the SEC-MALS data that the R141E/A306F variant showed concentration-dependent changes in retention time, which are reflected in its molecular mass (Table S4 of the Supporting Information).

Figure 5 provides a ready comparison of the AUC and SEC-MALS data for *wt* BFDC and the two variants, R141E/A306F and R141E/Y288A/A306F. The continuous size distribution analysis data, obtained at a protein concentration of 0.5 mg/mL (8.6 μM), highlight the trend toward lower *S* values, indicative of a smaller species. In addition, at 0.75 mg/mL, both variants have a clear increase in retention time over that of *wt* BFDC (Figure 5B), confirming a movement toward dimer formation.

Equilibrium Denaturation Measurements. The urea-mediated unfolding of *wt* BFDC and the R141E/A306F variant was followed by both intrinsic fluorescence and CD spectroscopy. To highlight any differences, the unfolding experiments were conducted at an enzyme concentration of 0.15 mg/mL. At this concentration, the *wt* enzyme is tetrameric whereas the R141E/A306F variant is expected to be primarily dimeric. As shown in Figure 6A, when monitored using the intrinsic fluorescence signal at 327 nm, the unfolding of *wt* BFDC appears to have three transitions. Initially, between 0 and 0.5 M urea, there is a small increase in fluorescence. Another small transition is observed on going from 0.5 to 2 M urea, while the largest transition takes place between 2 and 6 M urea. Potentially, the first corresponds to the dissociation of tetramers to dimers; the second is that of the dimers to monomers, and the third results from the unfolding of the monomers. Such a pattern was also observed for *Sc*PDC.[25] By contrast, the unfolding of the R141E/A306F variant showed only two transitions (Figure 6A), most likely due to the initial unfolding of the dimer followed by unfolding of the monomer.

Similar results were observed for *wt* BFDC when unfolding was monitored by far UV-CD (Figure 6B). Further, the urea-induced inactivation of *wt* BFDC is complete by 3.5 M urea (Figure 6B), and it is evident that some degree of inactivation of the *wt* enzyme has occurred even at urea concentrations as low as 0.25 M. This decrease in the activity of *wt* BFDC is presumably caused by the dissociation of the tetramer. This result is in stark contrast to that found in the same experiment conducted with *Sc*PDC. In that case, the enzyme was fully active at 1 M urea, and dimers and tetramers were equally active.[25] The unfolding of the

dx.doi.org/10.1021/bi500081r | *Biochemistry* 2014, 53, 4358−4367

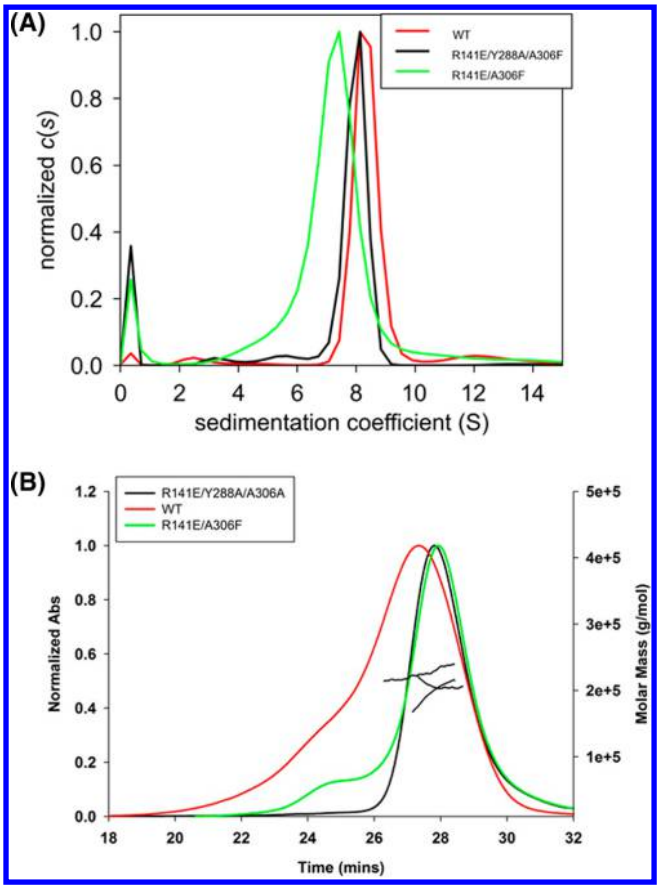

Figure 5. (A) Distribution of normalized $c(s)$ values for *wt* BFDC and the R141E/A306F and R141E/Y288A/A306F variants. In each case, the protein concentration was 0.5 mg/mL (8.6 μM). At that concentration, the *S* values are 8.4, 7.9, and 7.3 for the *wt*, triple mutant, and double mutant, respectively. (B) SEC-MALS analysis of *wt* BFDC and the two variants (0.75 mg/mL) shows the change in the dimer−tetramer equilibrium for the latter.

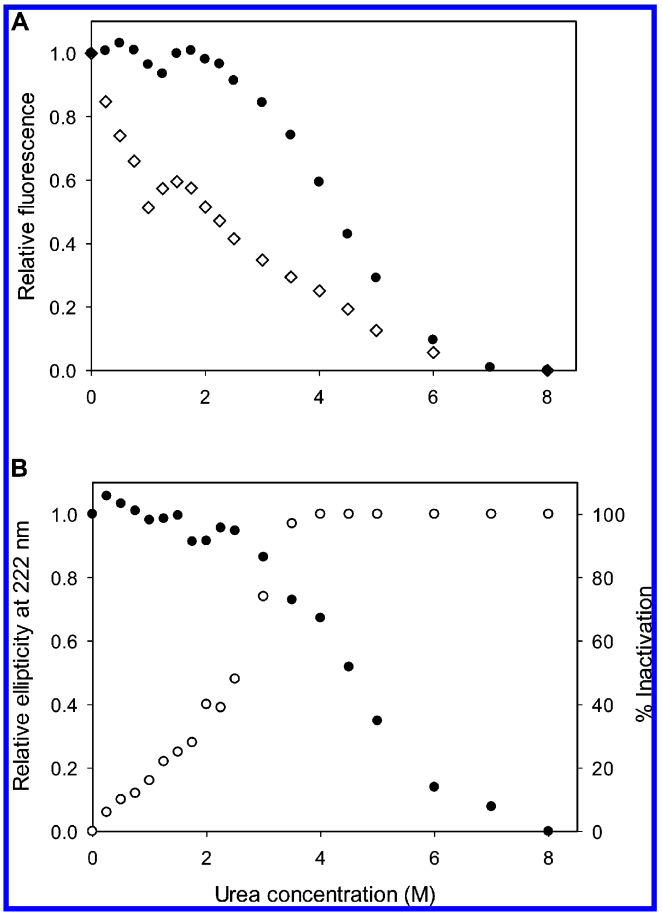

Figure 6. Equilibrium unfolding of BFDC by urea. (A) Relative changes in intrinsic fluorescence at 327 nm (λ_{ex} at 280 nm) for *wt* BFDC (●) and the R141E/A306F variant (◇). (B) Relative changes in ellipticity at 222 nm (●) and enzymatic activity (○) for *wt* BFDC. All changes were monitored at 20 °C. The results shown are the average of at least two independent measurements.

R141E/A306F variant, monitored by CD, followed a pattern almost identical to that observed in the fluorescence experiments (Figure S3 of the Supporting Information). Unfortunately, because of low levels of activity, it was not possible to follow the inactivation of the R141E/A306F variant. Nonetheless, the experiments did demonstrate clearly that there were distinct differences in the urea-mediated denaturation of *wt* BFDC and the R141E/A306F variant, providing additional evidence that the equilibrium has shifted toward dimer formation in the latter.

X-ray Structures of the R141E and A306F Variants. Attempts to crystallize the double and triple variants were unsuccessful. However, the X-ray structures of the R141E (PDB entry 4MPR) and A306F (PDB entry 4MQ5) variants were determined to resolutions of 1.40 and 1.50 Å, respectively (Table 3). Both exhibited the same fold as the *wt* enzyme; their space group and cell dimensions were also identical, and as previously observed with other BFDC structures, residues 461−468 had the highest *B* factors of any region of the protein.[18,42] The active sites were also unchanged, and given that the kinetic parameters for these variants were similar to those of *wt* BFDC (Table 2), this result was not entirely unexpected. However, the mutations did bring about some unanticipated structural changes that are worthy of comment.

It was predicted that mutating Arg141 to a glutamate would result in a variant that not only would be unable to form a salt bridge with Glu107 but also would create like-charge repulsion between Glu107 and Glu141. Surprisingly, the crystal structure of the R141E variant revealed the carboxylate group of Glu141 is complexed to a Na^+ ion, as well as the indole moiety of Trp125 (Figure 7). Four water molecules were also coordinated to the sodium ion, as was the carbonyl of Gly105. One of these waters was located within 3 Å of the carboxylate of Glu107. It seems that these unexpected interactions were sufficient to alleviate the predicted charge−charge repulsion that was expected to tilt the equilibrium toward the dimeric state.

Perhaps the most surprising observation was that the A306F substitution resulted in the displacement of the side chain of Arg141. This meant that the guanidinium group of arginine forms an intramonomer salt bridge with the side chain of Glu134 rather than the intermonomer interaction with Glu107 (Figure 8). The net result was that the additional bulk of the new phenylalanine residue was readily accommodated.

DISCUSSION

In his structure-based analysis of the domain relationships inherent to the ThDP-dependent enzymes, Duggleby[12] proposed that the original enzyme was a protein that contained binding sites for both ends of the ThDP molecule. Dimerization provided an advance by which the intrinsic activity of the cofactor was enhanced. Duplication of the gene for the primitive

dx.doi.org/10.1021/bi500081r | *Biochemistry* 2014, 53, 4358−4367

Table 3. Data, Model, and Crystallographic Statistics for the Structures of R141E and A306F BFDC

	R141E BFDC[a]	A306F BFDC[b]
	Data Collection[c]	
beamline	APS, GM/CA-CAT, 23-ID-D	APS, GM/CA-CAT, 23-ID-B
wavelength (Å)	1.03	1.03
space group	I_{222}	I_{222}
cell constants	a = 80.98 Å	a = 81.63 Å
	b = 95.97 Å	b = 95.54 Å
	c = 137.3 Å	c = 137.6 Å
	$\alpha = \beta = \gamma = 90°$	$\alpha = \beta = \gamma = 90°$
no. of unique reflections	104731	85254
resolution limit (Å)	1.40 (1.40−1.45)	1.50 (1.50−1.53)
completeness (%)	99.8 (99.8)	99.4 (100)
redundancy	7.2 (7.1)	5.2 (5.0)
$I/\sigma I$	27 (2.9)	46 (8.7)
R_{merge} (%)	8.5 (78)	5.0 (24)
	Refinement	
resolution range (Å)	1.40−48.0	1.50−26.4
R_{free} test set size	1997	2000
R_{cryst} (%)	12.45	11.96
R_{free} (%)	14.96	14.72
no. of atoms		
total	4738	4730
protein	4116	4108
water	591	591
overall B factor	12.15	12.78
rmsd		
bond lengths (Å)	0.015	0.009
bond angles (deg)	1.563	1.289

[a]PDB entry 4MPR. [b]PDB entry 4MQ5. [c]Value in parentheses are for the highest-resolution shell.

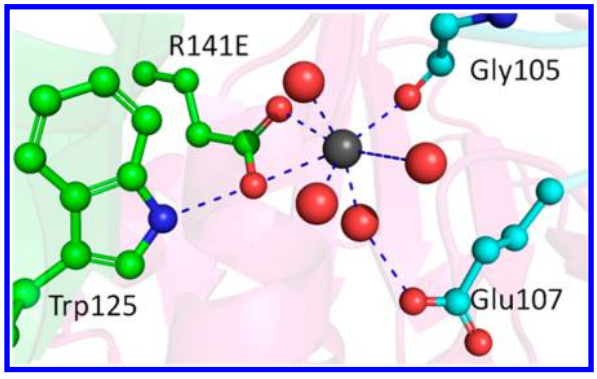

Figure 7. Potential Glu141−Glu107 interaction avoided in the R141E variant. Instead, Glu141 is found coordinated to Trp125 and an additional Na^+ ion. Blue dashes indicate distances of ≤3 Å.

decarboxylase resulted in an $\alpha_2\beta_2$ heterotetramer, likely a still more efficient enzyme. Subsequently, gene fusion led to the combination of the PP and PYR domains, giving rise to, effectively, an $(\alpha\beta)_2$ protein that can be seen to this day in phosphonopyruvate decarboxylase.[12,43] The more modern ThDP-dependent decarboxylases at some point acquired a third domain, the TH3 domain, which fused between the PYR and PP domains.[12] A broadly similar evolutionary pattern has also been postulated on the basis of sequence analysis, with the added suggestion that recruitment of the TH3 domain was accompanied by tetramer formation.[13]

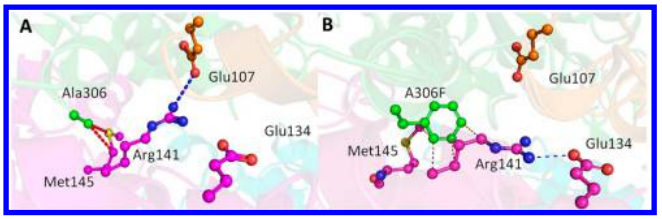

Figure 8. A306F variant provided an unexpected rearrangement in the A−D interface. (A) *wt* BFDC showing the original positions of Met145 and Arg141. (B) Phe306 causes Met145 and Arg141 to adopt new rotamers, the latter stabilized by interaction with Glu134. Blue dashes indicate a distance of ∼3 Å. Red dashes indicate distances of ≤4 Å.

What was not considered in any of these discussions is whether tetramer formation is essential or, if not, what advantage accrues due to tetramer formation. Allosteric regulation may have been a possible candidate, particularly as KdcA is a dimer and exhibits Michaelis−Menten kinetics whereas *Sc*PDC is subject to allosteric activation by its substrate.[44] However, this explanation is made less likely by the X-ray structures of *Sc*PDC in its unliganded[45] and substrate-activated forms,[46] which both show the enzyme to be tetrameric. Further, studies by Killenberg-Jabs et al.[24,25] have found that *Sc*PDC exists as an equilibrium mixture of dimers and tetramers under physiological conditions, and that there was no difference in the steady-state activity between the two states. Altogether, it would appear that the ability to form a tetramer is not a prerequisite for allosteric activation.

In contrast to *Sc*PDC, BFDC is tetrameric and obeys Michaelis−Menten kinetics. In many ways, it is more comparable to the PDC from *Zymomonas mobiliz* (*Zm*PDC), which has similar properties.[17] The similarity was confirmed by SPPIDER analysis, which showed that an individual monomer in both BFDC and *Zm*PDC makes significant contact with the other three monomers in the tetramer (Table 1). This is quite different from the cases of KdcA and *Sc*PDC, which show contacts only between the two monomers comprising the catalytic dimer.

Attempts to alter the dimer−tetramer equilibrium of BFDC by disrupting the noncatalytic monomer−monomer interfaces with point mutations were unsuccessful. Initially, it took the introduction of three mutations before any change was observed by SEC. This shift in equilibrium was confirmed by analytical ultracentrifugation. The R141E/Y288A/A306F variant showed no activity in the standard assay or in those containing 500 μg/mL enzyme. Subsequently, it was shown that two mutations, R141E and A306F, were sufficient to alter the dimer−tetramer equilibrium. At an assay concentration of 40 μg/mL, this variant showed a considerable (∼450-fold) reduction in its k_{cat} from that of *wt* BFDC, but it was impossible to say whether this was a reflection of the presence of tetramer in solution or the dimer indeed retained some activity. To investigate the latter possibility, we turned to equilibrium denaturation experiments.

It has been shown that, in a 0.5 M urea solution, *Sc*PDC forms dimers, and those dimers have the same specific activity as the tetramers.[24] Here we found that BFDC has a urea unfolding curve similar to that of *Sc*PDC, regardless of whether unfolding was measured by intrinsic fluorescence or by CD. However, unlike *Sc*PDC, BFDC showed a rapid loss of activity, even at urea concentrations as low as 0.25 M. Taken together, our data suggest that, to be catalytically active, it is necessary for BFDC to be a tetramer.

dx.doi.org/10.1021/bi500081r | *Biochemistry* 2014, 53, 4358−4367

Although that may be a reasonable conclusion, it is still not clear why the tetramer is necessary. Although all the single variants were very active, indicating that they were still tetrameric, the X-ray structures of both R141E and A306F provided some clues, with the most insightful piece of information coming from the crystal structure of the A306F variant. It was predicted that replacing Ala306 with phenylalanine would result in a steric clash that would help destabilize the tetramer. Surprisingly, the A306F structure revealed a rearrangement of the shallow pocket, by which the additional steric bulk of the phenylalanine was accommodated (Figure 8). This was due to the displacement of the side chain of Arg141 and Met145, which resulted in a larger binding pocket. The new rotamer of Arg141 saw the loss of the intermonomer interaction with Glu107 and the formation of a new intramonomer bond with Glu134 (Figure 8). Extrapolating to the R141E/A306F variant, we could assume that rather than Glu141 forming a salt bridge with Glu134, the interaction would be unfavorable. Potentially, this could cause Glu141 to spring back into its "original" position, making the accommodation of Phe306 more difficult. In the R141E structure, the enzyme used an additional sodium ion to help adapt to the potential Glu107−Glu141 contact (Figure 7). This may not be feasible in the R141E/A306F variant. The net result would be that the A−C and A−D interfaces are both destabilized, pushing the equilibrium toward the dimer as suggested by the SEC and equilibrium denaturation experiments.

Again, this is speculation, and it does not provide any insight into the apparent necessity for BFDC to be tetrameric to be catalytically active. Still, it is possible to take the speculation a little further by looking more closely at structural differences among BFDC, KdcA, and PDC. The three all belong to the decarboxylase-like (DC) structural clade of ThDP-dependent enzymes.[12] The vast majority of enzymes of the DC clade possess an inner active site loop that contains residues known to be critical to their catalytic mechanism. For example, the loops of *Sc*PDC, 3-indole-pyruvate decarboxylase, phenylpyruvate decarboxylase, and KdcA all include two adjoining histidine residues sometimes termed the HH motif.[47] Mutagenesis of either histidine results in a decrease in catalytic activity of orders of magnitude.[48−50] Conversely, although the active site of BFDC also contains two catalytically important histidine residues, these are not located on the inner loop. Instead, the loop of BFDC houses two contiguous leucine residues, Leu109 and Leu110. Alignment of the sequences of enzymes annotated as BFDCs in the thiamin enzyme engineering database (TEED) shows that Leu110 is completely conserved, and that leucine, or another hydrophobic residue, is invariably found at position 109.[51]

Examination of the X-ray structure of BFDC in complex with benzoyl phosphonic acid methyl ester (MBP), an analogue of benzoylformate, shows that Leu109 lines the phenyl-binding pocket of BFDC and that Leu110 has five points of contact within 5 Å of the glyoxylate analogue portion of MBP (Figure 9). From this structure, it appears that Leu110 acts as a clamp to lock the glyoxylate moiety into the perpendicular arrangement of the carboxylate group to the thiazolium−C2α bond. This geometry is thought to promote decarboxylation by allowing the maximal overlap of the π electrons of the thiazolium ring and the p orbital of the scissile bond.[52,53] Intriguingly, the active site loop of BFDC is bookended by Glu107 and Asp114, which, of course, interact with Arg141 and Arg120, respectively, in the A−C interface (Figure 4). It is not unreasonable to imagine that these two salt bridges may be responsible for maintaining the correct positioning of Leu109 and Leu110 within the active site of

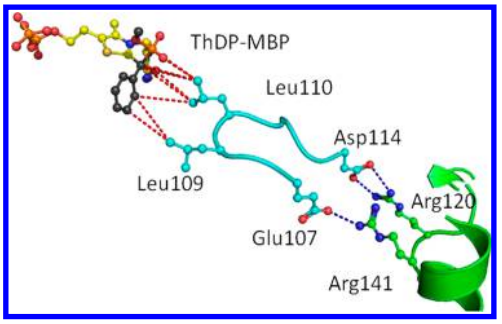

Figure 9. Leu109 and Leu110 are positioned by the interaction of Arg141 and Arg120 of monomer A with Glu107 and Asp114 of monomer C, respectively. Blue dashes indicate distances of ∼3 Å. Red dashes indicate distances of ≤5 Å.

BFDC, thereby contributing to both the overall hydrophobicity of the active site and the correct position of the substrate within it.

To assess the importance of the two leucine residues, both Leu109 and Leu110 were replaced, in turn, with alanine. Both variants showed decreases in k_{cat} of 2 orders of magnitude, while L110A also exhibited a 9-fold increase in K_m (Table 2). Overall, the changes were broadly in line with those observed with the R141E/A306F variant. It would appear that the decrease in activity observed with the latter may be due to movement in the inner loop resulting in the misalignment of Leu109 and Leu110 within the active site. To test this assumption, the E107R/D114R double variant was generated to completely disrupt the A−C interface, simultaneously preventing the correct positioning of both Leu109 and Leu110. While the individual substitutions produced only a modest effect on catalysis, the catalytic efficiency of the E107R/D114R variant was ∼600-fold lower than that of *wt* BFDC (Table 2). It is notable that the k_{cat} and K_m values for this variant were very similar to those of R141E/A306F, yet SEC data suggested that the E107R/D114R variant remained a tetramer. On that basis, it may be that the integrity of the dimer interface, rather than the tetrameric structure per se, is of paramount importance.

CONCLUSION

We have demonstrated that, in some cases, only two point mutations are required to alter the dimer−tetramer equilibrium of BFDC. In addition, it is apparent that the shift in equilibrium toward dimer formation is accompanied by a loss of catalytic activity. Finally, we provide evidence that suggests the tetrameric structure of BFDC has evolved as a means of positioning and stabilizing the active site loop residues, Leu109 and Leu110.

ASSOCIATED CONTENT

Supporting Information

A summary of monomer−monomer interactions, sequences of primers, analytical centrifugation and SEC-MALS analysis, and the urea unfolding curve of the R141E/A306F variant monitored by CD. This material is available free of charge via the Internet at http://pubs.acs.org.

AUTHOR INFORMATION

Corresponding Author

*Department of Chemistry and Chemical Biology, Indiana University-Purdue University Indianapolis, 402 N. Blackford St., Indianapolis, IN 46202. E-mail: mcleish@iupui.edu. Telephone: (317) 274-6889. Fax: (317) 274-4701.

Funding

This work was supported, in part, by National Science Foundation Grants EF-0425719 and CHE-1306877 (M.J.M.). The AUC studies were supported by a Project Development Team within ICTSI NIH/NCRR Grant TR000006. Use of the Advanced Photon Source, an Office of Science User Facility operated for the U.S. Department of Energy (DOE) Office of Science by Argonne National Laboratory, was supported by the U.S. DOE under Contract DE-AC02-06CH11357. GM/CA @ APS has been funded in whole or in part with Federal funds from the National Cancer Institute (Y1-CO-1020) and the National Institute of General Medical Sciences (Y1-GM-1104).

Notes

The authors declare no competing financial interest.

■ ACKNOWLEDGMENTS

We thank Malea Kneen for helping with reading and editing of the manuscript. We also thank the reviewers for their critical reading of the manuscript. Their comments pointed us to an error in a figure that subsequently lead to an erroneous interpretation. The paper is significantly better for their efforts.

■ ABBREVIATIONS

ThDP, thiamin diphosphate; BFDC, benzoylformate decarboxylase; PDC, pyruvate decarboxylase; *Sc*PDC, pyruvate decarboxylase from *S. cerevisiae*; AUC, analytical ultracentrifugation; BSA, bovine serum albumin; CD, circular dichroism; HLADH, horse liver alcohol dehydrogenase; SEC, size-exclusion chromatography; SEC-MALS, size-exclusion chromatography multiangle light scattering; *wt*, wild-type.

■ REFERENCES

(1) Ryan, D. P., and Matthews, J. M. (2005) Protein−protein interactions in human disease. *Curr. Opin. Struct. Biol. 15*, 441−446.

(2) Meiering, E. M. (2008) The threat of instability: Neurodegeneration predicted by protein destabilization and aggregation propensity. *PLoS Biol. 6*, e193.

(3) Blake, D. J., Weir, A., Newey, S. E., and Davies, K. E. (2002) Function and genetics of dystrophin and dystrophin-related proteins in muscle. *Physiol. Rev. 82*, 291−329.

(4) Rual, J. F., Venkatesan, K., Hao, T., Hirozane-Kishikawa, T., Dricot, A., Li, N., Berriz, G. F., Gibbons, F. D., Dreze, M., Ayivi-Guedehoussou, N., Klitgord, N., Simon, C., Boxem, M., Milstein, S., Rosenberg, J., Goldberg, D. S., Zhang, L. V., Wong, S. L., Franklin, G., Li, S., Albala, J. S., Lim, J., Fraughton, C., Llamosas, E., Cevik, S., Bex, C., Lamesch, P., Sikorski, R. S., Vandenhaute, J., Zoghbi, H. Y., Smolyar, A., Bosak, S., Sequerra, R., Doucette-Stamm, L., Cusick, M. E., Hill, D. E., Roth, F. P., and Vidal, M. (2005) Towards a proteome-scale map of the human protein-protein interaction network. *Nature 437*, 1173−1178.

(5) Cusick, M. E., Klitgord, N., Vidal, M., and Hill, D. E. (2005) Interactome: Gateway into systems biology. *Hum. Mol. Genet. 14*, R171−R181.

(6) Ho, E., Webber, R., and Wilkins, M. R. (2008) Interactive three-dimensional visualization and contextual analysis of protein interaction networks. *J. Proteome Res. 7*, 104−112.

(7) Gough, C. A., Homma, K., Yamaguchi-Kabata, Y., Shimada, M. K., Chakraborty, R., Fujii, Y., Iwama, H., Minoshima, S., Sakamoto, S., Sato, Y., Suzuki, Y., Tada-Umezaki, M., Nishikawa, K., Imanishi, T., and Gojobori, T. (2012) Prediction of protein-destabilizing polymorphisms by manual curation with protein structure. *PLoS One 7*, e50445.

(8) Zhang, Q. C., Petrey, D., Deng, L., Qiang, L., Shi, Y., Thu, C. A., Bisikirska, B., Lefebvre, C., Accili, D., Hunter, T., Maniatis, T., Califano, A., and Honig, B. (2012) Structure-based prediction of protein-protein interactions on a genome-wide scale. *Nature 490*, 556−560.

(9) Valencia, A., and Pazos, F. (2002) Computational methods for the prediction of protein interactions. *Curr. Opin. Struct. Biol. 12*, 368−373.

(10) Marianayagam, N. J., Sunde, M., and Matthews, J. M. (2004) The power of two: Protein dimerization in biology. *Trends Biochem. Sci. 29*, 618−625.

(11) Ali, M. H., and Imperiali, B. (2005) Protein oligomerization: How and why. *Bioorg. Med. Chem. 13*, 5013−5020.

(12) Duggleby, R. G. (2006) Domain relationships in thiamine diphosphate-dependent enzymes. *Acc. Chem. Res. 39*, 550−557.

(13) Costelloe, S. J., Ward, J. M., and Dalby, P. A. (2008) Evolutionary analysis of the TPP-dependent enzyme family. *J. Mol. Evol. 66*, 36−49.

(14) Pohl, M., Sprenger, G. A., and Müller, M. (2004) A new perspective on thiamine catalysis. *Curr. Opin. Biotechnol. 15*, 335−342.

(15) Schneider, G., and Lindqvist, Y. (1998) Crystallography and mutagenesis of transketolase: Mechanistic implications for enzymatic thiamin catalysis. *Biochim. Biophys. Acta 1385*, 387−398.

(16) Lu, G., Dobritzsch, D., Baumann, S., Schneider, G., and König, S. (2000) The structural basis of substrate activation in yeast pyruvate decarboxylase. *Eur. J. Biochem. 267*, 861−868.

(17) Dobritzsch, D., König, S., Schneider, G., and Lu, G. (1998) High resolution crystal structure of pyruvate decarboxylase from *Zymomonas mobilis*. Implications for substrate activation in pyruvate decarboxylases. *J. Biol. Chem. 273*, 20196−20204.

(18) Hasson, M. S., Muscate, A., McLeish, M. J., Polovnikova, L. S., Gerlt, J. A., Kenyon, G. L., Petsko, G. A., and Ringe, D. (1998) The crystal structure of benzoylformate decarboxylase at 1.6 Å resolution: Diversity of catalytic residues in thiamin diphosphate-dependent enzymes. *Biochemistry 37*, 9918−9930.

(19) Berthold, C. L., Moussatche, P., Richards, N. G. J., and Lindqvist, Y. (2005) Structural basis for activation of the thiamin diphosphate-dependent enzyme oxalyl-CoA decarboxylase by adenosine diphosphate. *J. Biol. Chem. 280*, 41645−41654.

(20) Versees, W., Spaepen, S., Vanderleyden, J., and Steyaert, J. (2007) The crystal structure of phenylpyruvate decarboxylase from *Azospirillum brasilense* at 1.5 Å resolution. Implications for its catalytic and regulatory mechanism. *FEBS J. 274*, 2363−2375.

(21) Schütz, A., Sandalova, T., Ricagno, S., Hübner, G., König, S., and Schneider, G. (2003) Crystal structure of thiamindiphosphate-dependent indolepyruvate decarboxylase from *Enterobacter cloacae*, an enzyme involved in the biosynthesis of the plant hormone indole-3-acetic acid. *Eur. J. Biochem. 270*, 2312−2321.

(22) Berthold, C. L., Gocke, D., Wood, M. D., Leeper, F. J., Pohl, M., and Schneider, G. (2007) Structure of the branched-chain keto acid decarboxylase (KdcA) from *Lactococcus lactis* provides insights into the structural basis for the chemoselective and enantioselective carboligation reaction. *Acta Crystallogr. D63*, 1217−1224.

(23) Kutter, S., Spinka, M., Koch, M., and König, S. (2007) The influence of protein concentration on oligomer structure and catalytic function of two pyruvate decarboxylases. *Protein J. 26*, 585−591.

(24) Killenberg-Jabs, M., Jabs, A., Lilie, H., Golbik, R., and Hübner, G. (2001) Active oligomeric states of pyruvate decarboxylase and their functional characterization. *Eur. J. Biochem. 268*, 1698−1704.

(25) Killenberg-Jabs, M., Kern, G., Hübner, G., and Golbik, R. (2002) Folding and stability of different oligomeric states of thiamin diphosphate dependent homomeric pyruvate decarboxylase. *Biophys. Chem. 96*, 259−271.

(26) Hegeman, G. D. (1966) Synthesis of the enzymes of the mandelate pathway by *Pseudomonas putida* I. Synthesis of enzymes by the wild type. *J. Bacteriol. 91*, 1140−1154.

(27) Hegeman, G. D. (1970) Benzoylformate decarboxylase (*Pseudomonas putida*). *Methods Enzymol. 17*, 674−678.

(28) Siegert, P., McLeish, M. J., Baumann, M., Iding, H., Kneen, M. M., Kenyon, G. L., and Pohl, M. (2005) Exchanging the substrate specificities of pyruvate decarboxylase from *Zymomonas mobilis* and benzoylformate decarboxylase from *Pseudomonas putida*. *Protein Eng., Des. Sel. 18*, 345−357.

(29) Yep, A., and McLeish, M. J. (2009) Engineering the substrate binding site of benzoylformate decarboxylase. *Biochemistry 48*, 8387−8395.

(30) Andrews, F. H., Tom, A. R., Gunderman, P. R., Novak, W. R. P., and McLeish, M. J. (2013) A bulky hydrophobic residue is not required to maintain the V-conformation of enzyme-bound thiamin diphosphate. *Biochemistry 52*, 3028−3030.
(31) Yep, A., Kenyon, G. L., and McLeish, M. J. (2008) Saturation mutagenesis of putative catalytic residues of benzoylformate decarboxylase provides a challenge to the accepted mechanism. *Proc. Natl. Acad. Sci. U.S.A. 105*, 5733−5738.
(32) Kneen, M. M., Pogozheva, I. D., Kenyon, G. L., and McLeish, M. J. (2005) Exploring the active site of benzaldehyde lyase by modeling and mutagenesis. *Biochim. Biophys. Acta 1753*, 263−271.
(33) Gasteiger, E., Hoogland, C., Gattiker, A., Duvaud, S. E., Wilkins, M., Appel, R., and Bairoch, A. (2005) Protein identification and analysis tools on the ExPASy server. In *The Proteomics Protocols Handbook* (Walker, J. M., Ed.) pp 571−607, Humana Press, Totowa, NJ.
(34) Weiss, P. M., Garcia, G. A., Kenyon, G. L., Cleland, W. W., and Cook, P. F. (1988) Kinetics and mechanism of benzoylformate decarboxylase using carbon-13 and solvent deuterium isotope effects on benzoylformate and benzoylformate analogs. *Biochemistry 27*, 2197−2205.
(35) Schuck, P. (2000) Size-distribution analysis of macromolecules by sedimentation velocity ultracentrifugation and Lamm equation modeling. *Biophys. J. 78*, 1606−1619.
(36) Winn, M. D., Ballard, C. C., Cowtan, K. D., Dodson, E. J., Emsley, P., Evans, P. R., Keegan, R. M., Krissinel, E. B., Leslie, A. G. W., McCoy, A., McNicholas, S. J., Murshudov, G. N., Pannu, N. S., Potterton, E. A., Powell, H. R., Read, R. J., Vagin, A., and Wilson, K. S. (2011) Overview of the CCP4 suite and current developments. *Acta Crystallogr. D67*, 235−242.
(37) Adams, P. D., Afonine, P. V., Bunkoczi, G., Chen, V. B., Davis, I. W., Echols, N., Headd, J. J., Hung, L.-W., Kapral, G. J., Grosse-Kunstleve, R. W., McCoy, A. J., Moriarty, N. W., Oeffner, R., Read, R. J., Richardson, D. C., Richardson, J. S., Terwilliger, T. C., and Zwart, P. H. (2010) PHENIX: A comprehensive Python-based system for macromolecular structure solution. *Acta Crystallogr. D66*, 213−221.
(38) Emsley, P., and Cowtan, K. (2004) Coot: Model-building tools for molecular graphics. *Acta Crystallogr. D60*, 2126−2132.
(39) Davis, I. W., Murray, L. W., Richardson, J. S., and Richardson, D. C. (2004) MolProbity: Structure validation and all-atom contact analysis for nucleic acids and their complexes. *Nucleic Acids Res. 32*, W615−W619.
(40) Dyda, F., Furey, W., Swaminathan, S., Sax, M., Farrenkopf, B., and Jordan, F. (1993) Catalytic centers in the thiamin diphosphate dependent enzyme pyruvate decarboxylase at 2.4-Å resolution. *Biochemistry 32*, 6165−6170.
(41) Porollo, A., and Meller, J. (2007) Prediction-based fingerprints of protein−protein interactions. *Proteins: Struct., Funct., Bioinf. 66*, 630−645.
(42) Polovnikova, E. S., McLeish, M. J., Sergienko, E. A., Burgner, J. T., Anderson, N. L., Bera, A. K., Jordan, F., Kenyon, G. L., and Hasson, M. S. (2003) Structural and kinetic analysis of catalysis by a thiamin diphosphate-dependent enzyme, benzoylformate decarboxylase. *Biochemistry 42*, 1820−1830.
(43) Graupner, M., Xu, H., and White, R. H. (2000) Identification of the gene encoding sulfopyruvate decarboxylase, an enzyme involved in biosynthesis of Coenzyme M. *J. Bacteriol. 182*, 4862−4867.
(44) Hubner, G., Weidhase, R., and Schellenberger, A. (1978) The mechanism of substrate activation of pyruvate decarboxylase: A first approach. *Eur. J. Biochem. 92*, 175−181.
(45) Arjunan, P., Umland, T., Dyda, F., Swaminathan, S., Furey, W., Sax, M., Farrenkopf, B., Gao, Y., Zhang, D., and Jordan, F. (1996) Crystal structure of the thiamin diphosphate-dependent enzyme pyruvate decarboxylase from the yeast *Saccharomyces cerevisiae* at 2.3 Å resolution. *J. Mol. Biol. 256*, 590−600.
(46) Kutter, S., Weiss, M. S., Wille, G., Golbik, R., Spinka, M., and König, S. (2009) Covalently bound substrate at the regulatory site of yeast pyruvate decarboxylases triggers allosteric enzyme activation. *J. Biol. Chem. 284*, 12136−12144.
(47) Andrews, F. H., and McLeish, M. J. (2012) Substrate specificity in thiamin diphosphate-dependent decarboxylases. *Bioorg. Chem. 43*, 26−36.
(48) Schütz, A., Golbik, R., König, S., Hübner, G., and Tittmann, K. (2005) Intermediates and transition states in thiamin diphosphate-dependent decarboxylases. A kinetic and NMR study on wild-type indolepyruvate decarboxylase and variants using indolepyruvate, benzoylformate, and pyruvate as substrates. *Biochemistry 44*, 6164−6179.
(49) Liu, M., Sergienko, E. A., Guo, F., Wang, J., Tittmann, K., Hübner, G., Furey, W., and Jordan, F. (2001) Catalytic acid−base groups in yeast pyruvate decarboxylase. 1. Site-directed mutagenesis and steady-state kinetic studies on the enzyme with the D28A, H114F, H115F, and E477Q substitutions. *Biochemistry 40*, 7355−7368.
(50) Schenk, G., Leeper, F. J., England, R., Nixon, P. F., and Duggleby, R. G. (1997) The role of His113 and His114 in pyruvate decarboxylase from *Zymomonas mobilis*. *Eur. J. Biochem. 248*, 63−71.
(51) Widmann, M., Radloff, R., and Pleiss, J. (2010) The Thiamine diphosphate-dependent Enzyme Engineering Database: A tool for the systematic analysis of sequence and structure relations. *BMC Biochem. 11*, 9.
(52) Turano, A., Furey, W., Pletcher, J., Sax, M., Pike, D., and Kluger, R. (1982) Synthesis and crystal structure of an analog of 2-(alpha-lactyl)thiamin, racemic methyl 2-hydroxy-2-(2-thiamin)-ethylphosphonate chloride trihydrate. A conformation for a least-motion, maximum-overlap mechanism for thiamin catalysis. *J. Am. Chem. Soc. 104*, 3089−3095.
(53) Bruning, M., Berheide, M., Meyer, D., Golbik, R., Bartunik, H., Liese, A., and Tittmann, K. (2009) Structural and kinetic studies on native intermediates and an intermediate analogue in benzoylformate decarboxylase reveal a least motion mechanism with an unprecedented short-lived predecarboxylation intermediate. *Biochemistry 48*, 3258−3268.